Ground and Excited State Aromaticity in Azulene-Based Helicenes

Amisadai Lorenzo Reyes, Fatim Ndeye Ndiaye, Albert Artigas, Yoann Coquerel, Cyril Terrioux, Nicolas Prcovic, Denis Hagebaum-Reignier, Yannick Carissan

ChemPhysChem

Research Article
doi.org/10.1002/cphc.202400833

Chemistry Europe
European Chemical Societies Publishing

www.chemphyschem.org

Ground and Excited State Aromaticity in Azulene-Based Helicenes

Amisadai Lorenzo Reyes,*[a] Fatim Ndeye Ndiaye,[a] Albert Artigas,[b] Yoann Coquerel,[a] Cyril Terrioux,[c] Nicolas Prcovic,[c] Denis Hagebaum-Reignier,*[a] and Yannick Carissan*[a]

In honor of Prof. Solà for his 60th birthday.

Electron delocalization is studied in the ground singlet and first excited triplet states of azulene-containing helicenes. After showing that the compounds we study can be synthesized, we show that they exhibit a charge separation in the ground state, which does not appear in their triplet excited state. Then, magnetically induced properties (IMS3D and ACID) and electron density decomposition methods (EDDB) are used to rationalize aromaticity in these systems. For azulene-based helicenes larger than a critical size, that is, for more than six fused cycles, unexpected aromatic delocalization circuits appear. This feature is understood via the decomposition of the wavefunction on sets of carefully chosen local electronic structures and fragment orbital diagrams.

Introduction

The introduction of non-benzenoid units into nanographene structures has recently received particular attention due to the possibility of generating systems with a significant open-shell character, which may lead to the realization of future organic electronic and spintronic devices.[1–9] Azulene is an emblematic example of such non-alternant non-benzenoid polycyclic aromatic hydrocarbons (PAHs).[1,10–14] Azulene is a 10π-electron aromatic fused bicyclic hydrocarbon, isomer of naphthalene, with a dipole moment comparable to that of hydrogen chloride.[15] This unusual property results from the intramolecular interaction between a donor of a five-membered ring and a acceptor of a seven-membered ring, these donor / acceptor characters being driven by the $[4n+2]\pi$ Hückel's rule: the five-membered ring receives an electron from the seven-membered ring. Thus, the total delocalized wavefunction Ψ_{tot} can be written as the linear combination of two local wavefunctions ϕ_1 and ϕ_2:

$$\Psi_{tot} = c_1\phi_1 + c_2\phi_2 \quad (1)$$

In ϕ_1, six electrons are delocalized over the negatively charged five-membered ring, four electrons being delocalized over the remaining five carbon atoms. In ϕ_2, six electrons are delocalized over the positively charged seven-membered ring, four electrons being delocalized over the remaining three carbon atoms. This perspective has been questioned as the π-conjugation and/or electronic circulation across the transannular bond, computed with different descriptors, is weak, yielding conflicting results in terms of structure, magnetism, and related properties.[16,17] Azulene has been extensively studied, and its unique physicochemical and photophysical properties continue to attract considerable attention.[2,18,19]

Recently, azulene-embedded helicenes synthesis has been successfully achieved.[6,10,13,20–25] Helicenes, formed by orthoannulated aromatic rings, have contorted π systems and inherent chirality despite the absence of stereogenic centers. They possess attractive chiroptical properties, such as circular dichroism (CD) and circularly polarized luminescence (CPL).[26–29]

The combination of chirality with the peculiar photophysical properties of azulene[30] looks a promising strategy for the development of new chiroptical probes and sensors,[31] spin filters[32] or chiroptical switches.[33] In this direction, Li *et al.*[34] have provided a comparative theoretical study of azulene-containing tetracene and tetrahelicene and have shown the potentialities of the incorporation of azulene unit in the characteristics of the excited states (especially the reduction of the energy of the first excited triplet state) as a chromophore. The diradical character of the structures with small HOMO-LUMO gaps is also shown compared to that of their analogous benzenoid compounds without azulene units.

From a theoretical perspective, distorted polycyclic hydrocarbons question the old but still evolving concept of

[a] A. L. Reyes, F. N. Ndiaye, Y. Coquerel, D. Hagebaum-Reignier, Y. Carissan
Aix Marseille Univ, CNRS, Centrale Med, iSm2, Marseille, France
E-mail: amisadai.lorenzo-reyes@etu.univ-amu.fr
denis.hagebaum-reignier@univ-amu.fr
yannick.carissan@univ-amu.fr

[b] A. Artigas
Facultat de Ciències, Universitat de Girona, Campus Montilivi, Carrer de Maria Aurèlia Capmany i Farnès 69, 17003 Girona, Catalunya, Spain

[c] C. Terrioux, N. Prcovic
Aix Marseille Univ, CNRS, LIS, Marseille, France

Supporting information for this article is available on the WWW under https://doi.org/10.1002/cphc.202400833

aromaticity,[35–38] originally defined for the ground states of strictly planar π systems. As aromaticity is not an observable, there is no single accepted method for its study.

Energetic,[39] structural,[40,41] magnetic[42,43] and electron delocalization[44] criteria have been proposed to help understand the concept by using some physicochemical properties as a manifestation of aromaticity. This means that methods may occasionally yield conflicting results, requiring the combination of various criteria to approach the problem from different perspectives.[45–47]

The most relevant methods to characterize aromaticity in distorted molecules are based on the analysis of the electron density and its response to the application of an external magnetic field, with known limitations (see Computational Details section for detailed information).[47–49]

The analysis of the unperturbed electron density can be done using the EDDB (Electron Density of Delocalized Bonds) approach, which allows for the visualization of the electron density over multiple atoms.[50]

One of the most widely used tools to characterize aromaticity is the Nucleus-Independent Chemical Shift (NICS), proposed by Schleyer and coworkers.[41,42] NICS is a single value that represents the response to the magnetic field at a point in space. It does not give detailed information about the diatropic and paratropic flows, as well as about the local or global circuits.[49,51] It was shown to be challenging to apply to three-dimensional systems.[47,48] Based on the same concept of the response to an isotropic external magnetic field, three-dimensional visualization of Isotropic Magnetic Shielding (IMS3D) has been proposed by Artigas and co-workers,[52] which has allowed the straightforward visualization of electron delocalization in complex twisted systems.[53–56] The Anisotropy of the Induced Current Density (ACID) allows for the visualization of the electron flux induced by a non-isotropic external magnetic field.[57] Some approaches, based on valence bond theory, have been developed which consider the weight of the most relevant resonant structures and others based on the theory of molecular orbitals and their decomposition into localized molecular orbitals. Among the latter methods are those based on Natural Bond Orbital (NBO) developed by Weinhold et al.[58] The HLP (Hückel Lewis Projection) method was also developed for a decomposition of the delocalized wavefunction on a set of carefully chosen localized structures.[59]

Benzenoid helicene has been extensively studied, including comparisons with its acene and phenanthrene analogs, using various aromaticity descriptors.[60,61] In the present theoretical work we have substituted the terminal naphthalene unit or all naphthalene units of the three helical structures of interest, namely, tetrahelicene (**[4]-hel**), hexahelicene (**[6]-hel**), and octahelicene (**[8]-hel**), by azulene units. We name these compounds **[n]-hel-azu** and **[n]-azu** respectively, *n* is the total number of cycles. Among the possible fusion of azulene moieties with benzenoid units, we limit ourselves to compounds in which the fusion of azulenes occurs through their five-membered rings. This choice is driven by the recent synthesis of such compounds.[6,24] In addition, we analyzed the effect of increasing the number of azulene units on aromaticity when considering molecules containing 18, 26 and 34 π electrons corresponding to 4, 6, and 8 fused cycles, respectively. (Figure 1)

In this work, we are trying to answer four questions regarding the introduction of one or more azulene motifs in an helicene as described above. First, can these compounds be synthesized: are they stable? Second, does this modification create charge separation in the molecule? If so, what is the distance between the opposite charges? Does this charge separation also appear in the first triplet excited state? Then, does the wave function become more ionic, *i.e.* is described by ionic local structures, when doing such a modification? Finally, does this modification change the non-locality of the electron delocalization? If so, what is the new delocalization pattern to take into account. Different calculation methods are used to compare the aromaticity of the mono-substituted compounds (**[n]-hel-azu**) with the original helicenes and the full azulene helical structures (**[n]-azu**). We focus on the visualization of the aromaticity of the ground and the lowest triplet states, as well as the comparison of the gaps between both states for non-benzenoid fused derivatives with their respective benzenoid isomers. In order to understand the electronic structure of these compounds, we use a perturbative approach, which shows the frontier orbital interaction.

Computational Methods

Computational Details

All molecules were optimized at the B3LYP/6-311++G(d,p) level of theory using Gaussian 16 package.[62] Additionally, Grimme's dispersion with Becke and Johnson corrections was included (GD3BJ).[63—65] We ensure that these molecules are the minima of

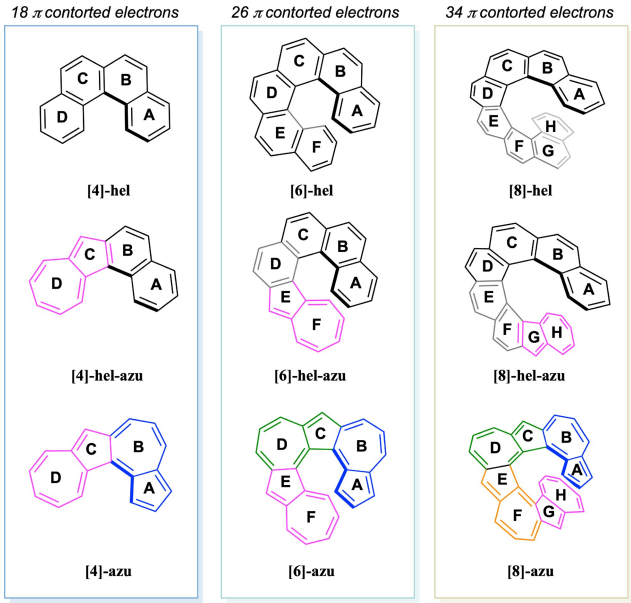

Figure 1. **[n]-hel**, **[n]-hel-azu** and **[n]-azu** compounds. Colors indicate azulene units and labelling of cycles will be used all along this work.

the potential energy surface by computing the analytical vibration frequencies, all of them being real positive.

IMS3D maps were computed at the same level of theory with the restricted or unrestricted formalism for S_0 and T_1, respectively. All maps were obtained using the ims3d.py program suite[52,66] with a depth value of 5 and a radius of 1 Å.

EDDB was carried out for the entire molecular system including hydrogen according to the latest version and procedure indicated by Szczepanik *et al.*,[50,67,68] using NBO7 version.[69] We chose to use the $EDDB_G$ flavour as the systems under study are not planar, hence with no σ/π separation, there seems to be no reason for not taking the electrons of the hydrogen atoms into consideration. The isosurfaces were obtained with an isovalue of 0.02.

ACID isosurfaces were generated for all electrons of the molecular system in each case, using version AICD-3.0.4,[57] for the isovalue of 0.05. For azulene, the external magnetic field was chosen to be perpendicular to the plane of the molecule pointing in the direction opposite to the reader. For non-planar molecules, the external field is perpendicular to the average molecular plane, i.e. the plane that minimizes the squared perpendicular distances of the atomic nuclei from it.

We computed the condensed NBO charges on all carbon atoms: each hydrogen carrying carbon atom is assigned its NBO charge to which the charge of the hydrogen it carries is added. Furthermore, when required, we have computed the charge of a cycle as the sum of the condensed charges of all its carbon atoms. Thus, we can assign a charge to each cycle. Note that these charges do not sum to the total charge of the system as the charge of atoms of a bond between two cycles are counted twice.

Electron Delocalization Analysis

We know that in distorted molecules, the σ/π separation is not strict as p_z orbitals of one atom are not orthogonal to *s* orbitals of its neighbors. Yet, one can assume that σ electrons keep being essentially σ, *i.e.* occupy molecular orbitals built as linear combinations of *s*, p_x and p_y orbitals, whereas π electrons keep being essentially π, *i.e.* occupy molecular orbitals built as linear combinations of p_z orbitals. Thus, in the following, when we write π-electrons, we mean *essentially* π*-electrons*.

In this work, we carefully selected three methods to characterize electron delocalization and aromaticity: EDDB, IMS3D and ACID. The EDDB approach, based on a decomposition of the total density, allows for the visualization of electron delocalization based on the natural bond orbital (NBO) theory performed on the stationary state. It allows for calculation of the number of delocalized electrons and easy visualization of the part of the electron density that is delocalized, *i.e.* spread over a set of bonds.

The IMS3D plots show the response of the electron density to an isotropic magnetic field, $\vec{B}_{iso}$. The trace of the shielding matrix, hence a scalar value, is plotted on the surface. Thus, this method is fully isotropic and fits the representation of aromaticity for 3D structures without specific directionality. The regions of the electron density that respond to $\vec{B}_{iso}$ by creating an opposing magnetic field are colored blue. This indicates aromaticity if the blue regions are cyclic. If the induced magnetic field reinforces $\vec{B}_{iso}$, regions are colored red and, if cyclic, indicate antiaromaticity. The darker the color, the stronger the aromatic/antiaromatic character, the less significant IMS values (corresponding to $|IMS| < 5.5$ ppm) are shown with the neutral beige color.

ACID plots are obtained by computing the response to $\vec{B}_{iso}$. The current induced by an oriented magnetic field $\vec{B}_{aniso}$ is represented by vectors plotted on the scalar surface, which represents the anisotropy of the response tensor to $\vec{B}_{iso}$. As this current is due to an anisotropic magnetic field, it requires that the systems for which it is plotted exhibit a specific orientation.

These visualization methods are accompanied, whenever necessary, by molecular orbital plots, spin densities as well as a Valence Bond description using localized Lewis structures. These structures are generated using a constraint programming algorithm that ensures the completeness of the set of structures. This constraint programming approach is solved using the choco solver. [70,71] Weights of the localized structures were obtained using the HuLiS software in the HLP formalism. [59,72] All inputs of wavefunction decomposition are available in a repository online.[73]

The combination of these approaches allows for the characterization of electron delocalization and aromaticity for non-planar molecules and rationalization of them whenever necessary.

Results and Discussion

Relative Stabilities

In Figure 2, we compare the relative stability of the singlet S_0 and triplet T_1 states of the **[n]-hel**, **[n]-hel-azu** and **[n]-azu** compounds with $n = 4$, 6 and 8. As can be seen and expected, for a given number of cycles n, the most stable helicene is the benzenoid helicene **[n]-hel**, followed by the **[n]-hel-azu** compound, the less stable being the **[n]-azu** compound (see Supporting Information SI.1). It is important to note here that all of these compounds are local minima of the potential energy surface. According to the extensive work of Mirzaei *et al.*,[74] the lowest energy pathway for the rearrangement of the azulene-naphthalene ring involves activation energies of at least 75 kcal/mol. The crossing of these barriers requires pyrolytic conditions. Therefore, these compounds cannot be easily isomerized under standard temperature conditions and are essentially stable. Similar azulene-containing compounds were recently synthesized, among them **[6]-hel-azu**.[20,24] This is clearly indicating that such molecules could be synthesized using appropriate methods.

From a thermodynamic point of view, azulene is 36.7 kcal/mol higher in energy than naphthalene.[74] This value is consistent with the energy differences we find between the **[n]-hel-azu** and **[n]-hel** compounds. Furthermore, it also agrees with the energy differences between the **[n]-hel** and **[n]-azu** compounds if we assume that the energy difference between them is due to $\frac{n}{2}$ isomerization (going from **[8]-azu** to **[8]-hel** requires 4 azulene to naphthalene isomerization).

Finally, we see that the singlet-triplet energy gap closes in the case **[n]-azu** with respect to increasing values of n, while it converges to a constant value for the compounds **[n]-hel** and **[n]-hel-azu**. This interesting behavior is due to the relative stability of the singlet and triplet states [75] which will be the subject of another study.

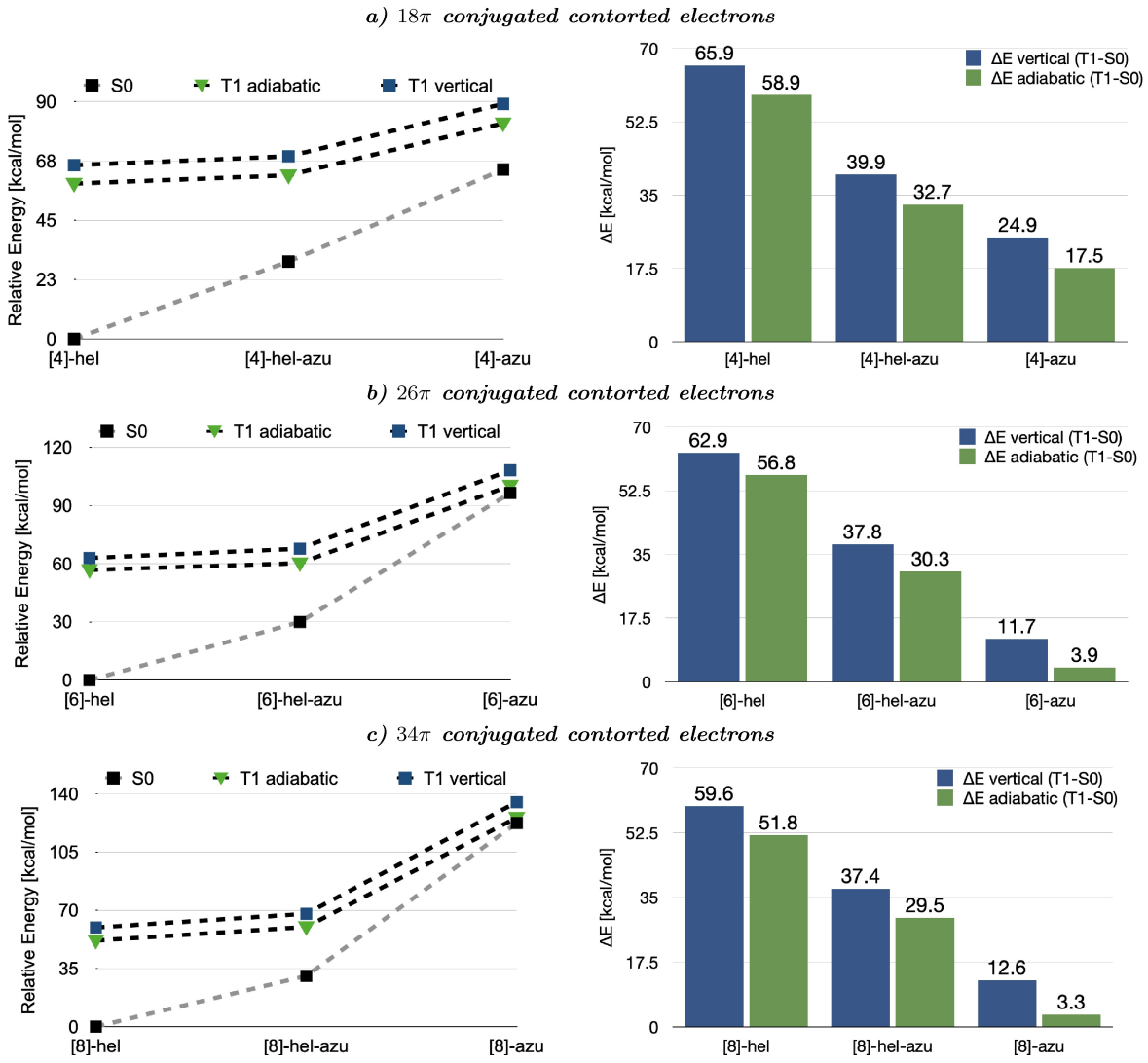

Figure 2. Relative stabilities of the singlet S_0 and triplet T_1 states (vertical and adiabatic ones) of the **[n]-hel**, **[n]-hel-azu** and **[n]-azu** compounds with $n = 4$, 6 and 8. The molecules are grouped according to the number of π electrons. The plots on the **left** show the energy values of the ground and triplet states relative to the S_0 state of **[n]-hel**. The histograms on the **right** show the energy difference between T_1 and S_0 states.

Intrinsic Properties of Azulene

Before studying the properties of azulene-based helicenes, it is informative to look at these properties for the azulene itself (see Figure 3).[17,76–79] When analyzing the charges, we notice that there is a negative charge shift toward the five-membered ring localized on carbons C13 and C17, as demonstrated experimentally through the greater nucleophilic character of these two carbons.[80,81] The singlet ground state exhibits aromaticity throughout the molecule (IMS3D), yet more localized on the five-membered ring (dark blue), whereas the excited triplet state shows a clear antiaromaticity (dark red). This is in line with the ACID map that clearly shows diatropic currents (clockwise) for the ground state and paratropic currents (counterclockwise) for the triplet state.

The EDDB analysis shown here is similar to the one obtained by Dunlop *et al.*:[17] in the ground state a global delocalization circuit appears on the perimeter, with no transannular delocalization, conversely the IMS map displays a clear delocalization in the transannular bond. In terms of ionicity of the states, the five-membered ring is negatively charged in the ground state and the seven-membered ring is positively charged, consistent with the existence of a dipole moment, whereas the dipole is reversed in the triplet state. The three aromaticity maps and the charge analysis show that the relaxed triplet state *i.e.* the triplet state in its optimized geometry ($T_{1\,\text{adiabatic}}$ in Figure 3) expresses a less antiaromatic character than the non-relaxed triplet (the triplet state in the geometry of the S_0 state $T_{1\,\text{vertical}}$). This illustrates the importance of considering optimized geometries in both the ground and excited states for comparative analysis. The EDDB isosurface patterns for $T_{1\,\text{adiabatic}}$ show a greater delocalization in the five-membered ring, particularly in the transannular bond, contrary to what is observed in the ground singlet state.

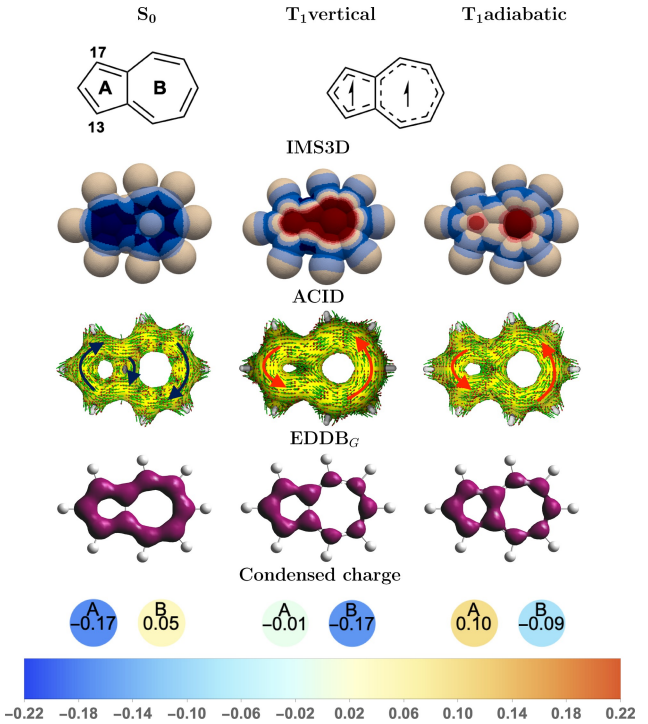

Figure 3. Comparison of aromaticity maps (IMS3D, ACID, EDDB$_G$) and NBO charges of azulene in its ground and first triplet excited states in terms of |e| units. For the ACID map, the external magnetic field points toward the reader, a red arrow indicates a paratropic current, and a blue arrow indicates a diatropic current (see Ref. [68] for high resolution ACID isosurfaces).

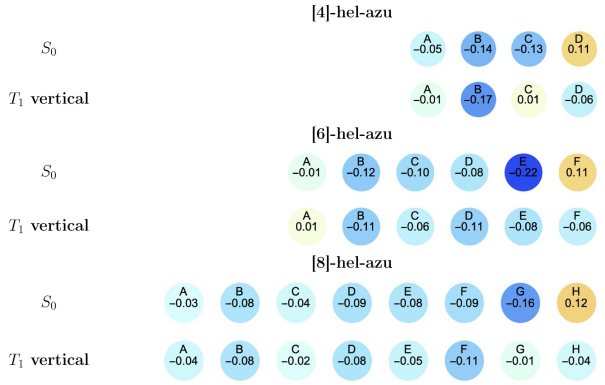

Figure 5. Ring-condensed NBO charges (in |e| unit) for the T_1 vertical triplet and S_0 ground states of **[n]-hel-azu** compounds.

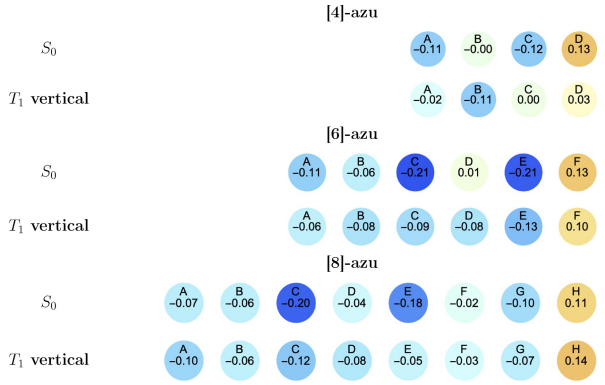

Figure 6. Ring-condensed NBO charges (in |e| unit) for the T_1 vertical triplet and S_0 ground states of **[n]-azu** compounds.

Charge Transfer and Dipole Moments Analysis in [n]-hel, [n]-hel-azu and [n]-hel-azu Compounds

In the light of the charge transfer observed for the azulene molecule, it is informative to analyze how this charge transfer is distributed among the fused rings in the **[n]-hel-azu** and **[n]-azu** compounds, as compared to the **[n]-hel** compounds. The results are summarized for the ground state and the vertical triplet state in Figures 4–6 (see Supporting Information SI.3.1 for the comparative results with the adiabatic triplet).

In this section, we shall analyze charges of each cycle of states S_0 and T_1 (vertical, adiabatic results are similar) of all helical compounds depicted in Figures 5–6. For **[n]-hel** compounds, all cycles are almost neutral, *i.e.* no cycle carries a meaningful charge independently of the state, contrary to compounds containing the azulene pattern. In the **[n]-hel-azu** cases, one sees a clear difference between the singlet and triplet states: the singlet state exhibits a non-negligible charge transfer within the azulene moiety. For the triplet, the picture resembles the **[n]-hel** case, *i.e.* cycles are neutral. The behavior of the ground and excited states is similar to that of the azulene case alone: a charge transfer in S_0 and a neutral T_1. Finally, in the **[n]-azu** molecules, there is a charge transfer in both states, S_0 and T_1. However, the nature of charge transfer is different for both states. The ground states of **[n]-azu** show a similar charge distribution: the terminal seven-membered ring is charged positively (D, F and H for $n=4$, 6 and 8 respectively) and all but the first five-membered rings (C for $n=4$, C and E for $n=6$ and C, E and G for $n=8$), are charged negatively. One can note that the initial azulene pattern made of the A and B cycles in all cases exhibits no charge transfer. In the triplet state, only the terminal seven-membered ring is positively charged. The other cycles basically carry no charge.

From this study, we see that in the ground state of **[n]-hel-azu** compounds, the azulene motif has a polarity similar to that of azulene alone. We even see a small polarity inversion in the triplet state of **[4]-hel-azu**. In the singlets, the positive charge is

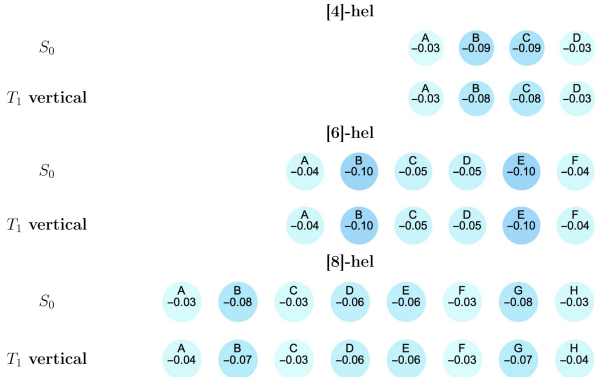

Figure 4. Ring-condensed NBO charges (in |e| unit) for the T_1 vertical triplet and S_0 ground states of **[n]-hel** compounds.

located on the seven-membered ring, and the negative charge is distributed over the other cycles.

For **[n]-azu** compounds, the distance between the positively charged seven-membered ring, *i.e.* rings D, F and H for **[4]-azu**, **[6]-azu** and **[8]-azu**, respectively, and the negatively charged five-membered ring increases with the size of the system. Surprisingly, the negative charge does not go all the way to the five-membered ring A opposite to the seven-membered ring. In the triplet state, the charge separation is tempered: the positive charge stays on the terminal seven-membered ring (in contrast to the azulene-only molecule) and the negative charge is evenly distributed among the remaining cycles.

Dipole Moments

The dipole moment depends on the partial charges of the individual atoms and their spatial arrangement. Table 1 presents its norm for each compound, and the spatial decomposition of each component is available in the Supporting Information SI.2.

As expected, the compounds with the highest dipole moment in S_0 are the azulene-based helicenes. Note that the helical distribution contributes to the increase in dipole moment, as can be seen in **[8]-hel** compared to **[4]**- and **[6]-hel**.

On the one hand, **[n]-hel-azu** compounds possess a dipole moment at S_0 that is similar to that of azulene. However, since the charge shifts less in T_1 than it does with azulene alone, there is a reduction in the dipole moment.

On the other hand, for **[n]-azu** ($n=6,8$) the dipole in T_1 remains the same as in the singlet state. This can be explained by the previously described charge distribution, where **[n]-azu** compounds retain negative and positive partial charges in T_1 for five- and seven-membered rings as well as in S_0.

Analysis in Terms of Localized Lewis Structures

To deepen our understanding of the wave function in the ground state, the total number of neutral structures was determined for each compound (Table 2).[71] They were then used to determine the trust factor to describe this state. This factor represents the quality of a given set of localized Lewis structures to describe the fully delocalized electronic wave function (Hückel level) of the considered molecule. It ranges from 0% (the set of structures is not relevant) to 100% (perfect match between the reference wave function and the set of localized structures).

Table 1. Dipole moments of the optimized geometries [Debye].

	S_0	T_1
Azulene	1.0746	0.5348
[4]-hel	0.0831	0.0878
[4]-hel-azu	1.0689	0.3906
[4]-azu	1.9453	0.6066
[6]-hel	0.0591	0.3887
[6]-hel-azu	1.1852	0.2938
[6]-azu	1.6321	1.0029
[8]-hel	0.2385	0.5787
[8]-hel-azu	1.1482	0.2088
[8]-azu	1.0962	1.6120

Table 2. Closed shell (CS) structures and trust factor for the wave function in the ground state of the wave function for each compound. The trust factor was only determined for $n=4$ and 6, due to the complexity of $n=8$ compounds due to their geometry, the number of atoms and the large number of local structures. The total number of CS structures was determined using choco solver algorithm and trust factor, τ, with HuLis software. Whenever possible the full set results are given. However, in some cases the projection procedure could not be performed due to redundancies between structures.

Compound	CS	τ	full set	τ	$\Delta\tau$
[4]-hel	8	34%	29	36%	+2
[4]-hel-azu	5	25%	23	29%	+4
[4]-azu	3	18%	30	25%	+7
[6]-hel	21	20%	–	–	
[6]-hel-azu	13	15%	–	–	
[6]-azu	4	7%	–	–	–
[8]-hel	55	–	–	–	
[8]-hel-azu	34	–	–		
[8]-azu	5	–	–	–	

As expected, due to their topology, benzenoid helicenes present a greater amount of neutral Lewis structures than azulene-based helicenes and also **[n]-hel-azu** compared to **[n]-azu**. The respective trust factors show that these closed shell structures describe **[4]-azu** and **[6]-azu** to a lesser extent (18% and 7% than their respective benzenoid analogues (34% and 20%). This points to a state with more diradical and/or ionic character when the azulene motif is introduced. If instead of considering only the neutral closed shell structures, diradical and ionic structures are included in the decomposition of the wave function (Table 2 full set) we see an increase of the trust factor, τ, larger for **[4]-azu** than for **[4]-hel-azu** and practically zero for **[4]-hel** compounds. Hence, the importance of radical and ionic structures in the wavefunction of azulene-containing compounds is demonstrated.

The wavefunction of **[4]-azu**, was decomposed over the set of the most important Lewis structures using HuLiS software.[82] As expected, the most important ones are non-radical neutral structures. However, many ionic structures have a more important weight than neutral diradical ones. Note that the six structures analyzed in Figure 7 span 25% of the total decomposition. This is relevant, as the other structures are extremely numerous, with a very small weight. Each ionic structure has a charge on a cycle, in agreement with its NBO condensed charge: negative on the five-membered rings and positive on the seven-membered rings.

In the triplet state, the same analysis is performed, Figure 7. Here again, we consider the most relevant structures, *i.e.* with

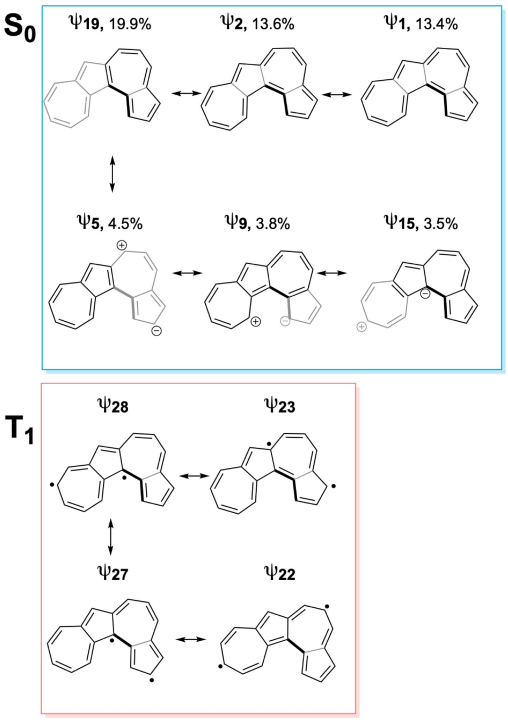

Figure 7. S_0, Six most meaningful Lewis structures (six highest weights) among the 30 most important of the decomposition of the ground state of **[4]-azu**. T_1, four diradical Lewis structures propose for the first triplet state for **[4]-azu**. (The diradical structures have the largest weight in the ground state according to HuLis were selected.)

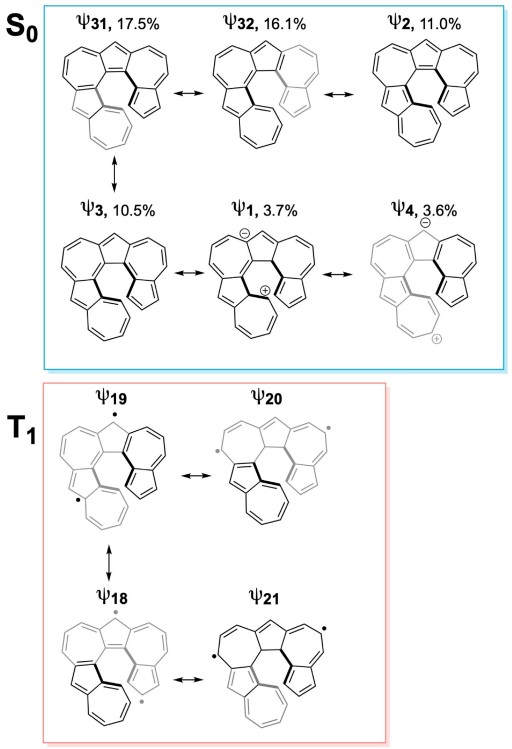

Figure 8. S_0, Six most meaningful Lewis structures (six highest weights) among the 24 most important of the decomposition of the ground state of **[6]-azu**. T_1, four diradical Lewis structures propose for the first triplet state for **[6]-azu**. (The diradical structures have the greatest weight in the ground state according to HuLis were selected.)

the highest weight. This state being diradical, the most important structures are diradicals.

Let us now consider the **[6]-azu** compound. The wave-function decomposition of S_0 (Figure 8) also reveals this predominant ionic character according to the weights of the structures investigated. The diradical structures, that in the ground state do not have a notable weight compared to the ionic ones, are more important (they were summarized from the highest to the least weight in the fundamental state, Figure 8) in the triplet state.

These qualitative results of the decomposition of wave-functions onto local Lewis structures will be connected to the electronic properties calculated in the following section.

Aromaticity Analysis in [n]-hel, [n]-hel-azu and [n]-azu Compounds

In the search to understand the nature of the ground state and first triplet excited state for azulene-based helicenes, IMS3D, ACID and EDDB maps will help us have a complementary vision.

[4]-hel, [4]-hel-azu and [4]-azu

The response to the applied magnetic field (Figure 9, IMS) of the electrons of the **[4]-hel** and **[4]-hel-azu** compounds in their

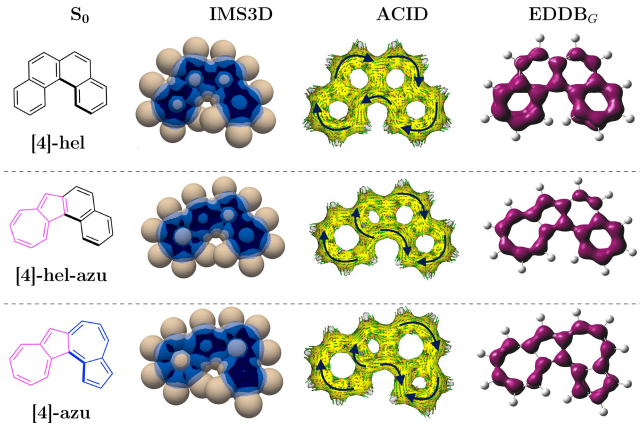

Figure 9. IMS-3D, ACID and EDDB for the singlet ground state of **[4]-hel**, **[4]-hel-azu** and **[4]-azu**. A red arrow indicates a paratropic current, and a blue arrow indicates a diatropic current (see Ref. [68] for high resolution ACID isosurfaces).

ground states are similar: aromaticity is spread throughout the entire skeleton, *i.e.* evenly on each cycle. Yet, when comparing the **[4]-hel** and **[4]-hel-azu**, we see a difference between the five- and seven-membered rings on one side, and their six-membered ring equivalents (*i.e.* at the same rank in the ring sequence) in the helicenes: the five-membered rings are more aromatic than their six-membered rings counterparts, whereas, the seven-membered rings are less aromatic than their six-

membered ring counterparts. This observation is in line with the description of the ground state of azulene in which the five-membered ring carries an overall negative charge.

In Figure 11, the π ACID plots using the set of $\{HOMO\text{-}i\}_{i=0,m}$ orbitals are represented. In each case, we chose *m* to best reproduce the ACID plot with all orbitals (Figures 9 and 10): the HOMO to HOMO-*m* orbitals are the most relevant orbitals to describe the response to the magnetic field. The ACID plot obtained with them allows for the reasonable withdrawal of the σ component from the all MO ACID plot.

This plot shows a current flowing at the periphery of the molecule: one does not distinguish any local circuit. This description matches the pictures obtained for the **[4]-hel**. ACID plots of singlet states of **[4]-hel-azu** and **[4]-azu** were compared and the description of aromaticity differs from **[4]-hel**. The full MO ACID plot shows the combination of two circuits: one local circuit, which implies three rings (5-7-5) and another local circuit, only on the terminal seven-membered ring. These circuits are to be considered disjoints, hence the azulene moiety does not behave as azulene alone (Figure 3). π ACID plots show that in the case of **[4]-azu** a greater number of orbitals is needed than in **[4]-hel** and **[4]-hel-azu**. This denotes the influence of quasi-degeneracy of orbitals close to the Fermi level for **[4]-azu**. This analysis also revealed that the electrons most susceptible to mobilization under an external magnetic field – observed in both the ACID and IMS3D methods – are those nearest to the Fermi level.

Let us now turn to the triplet states (Figure 10). IMS maps show regions with a predominant antiaromatic character in the internal rings for **[4]-hel** and in the terminal azulene motif for **[4]-hel-azu** and **[4]-azu**, less marked for **[4]-azu**. In particular, **[4]-hel-azu** shows some aromatic character in the terminal six-membered ring.

In this case the azulene part in **[4]-hel-azu** shows a clear antiaromatic circuit in all electron ACID plot. This circuit corresponds to MO number 61, which is the highest SOMO, Figure 11 (Supporting Information SI.6). We see that the azulene moiety behaves as azulene alone in this case. The images of the

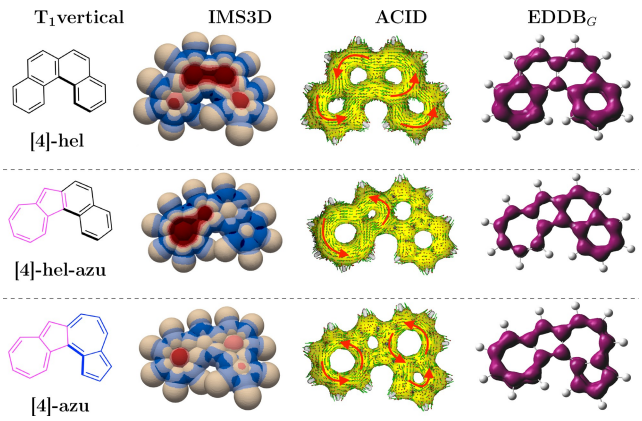

Figure 10. IMS-3D, ACID and EDDB for the vertical triplet state of **[4]-hel**, **[4]-hel-azu** and **[4]-azu**. A red arrow indicates a paratropic current, and a blue arrow indicates a diatropic current (see Ref. [68] for high resolution ACID isosurfaces).

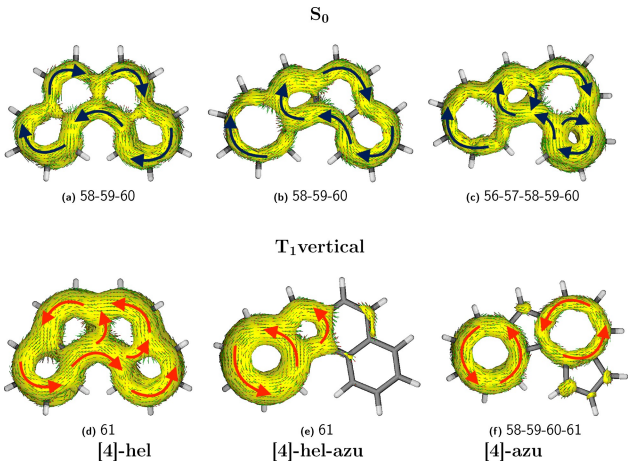

Figure 11. ACID plot of the selected σ/π orbitals close to the Fermi level for both singlet and vertical triplet states. In all cases 60th and 61th orbitals are the HOMO for S_0 and T_1, respectively. (a) and (d) correspond to **[4]-hel** compounds; (b) and (e) to **[4]-hel-azu**; and (c) and (f) to **[4]-azu**. Isovalue: 0.03.

[4]-azu molecule, both for the full MO ACID and the π MO ACID, reveal an antiaromatic region localized on the seven-membered rings, rather than on the individual azulene motifs. This antiaromatic region arises from the four highest molecular orbitals, in contrast to **[4]-hel** and **[4]-hel-azu** for which SOMO alone was sufficient to reproduce the full electron picture. Here again we state that the azulene moiety does not behave as azulene alone in **[4]-azu**.

EDDB analysis shows that electron delocalization in the stationary singlet and triplet states of **[4]-hel**, **[4]-hel-azu** and **[4]-azu** occurs along a path, which involves all carbon atoms at the periphery of the molecule. However, it is notable that the π only ACID plots for the triplet states of **[4]-hel-azu** and **[4]-azu** involve a limited number of occupied orbitals. This local behavior should be noted and cannot be seen using EDDB alone. This is because EDDB shows properties of the unperturbed state, whereas ACID shows the response of the electron cloud to the application of the external field. To understand why the **[4]-azu** compound behaves differently from the compound **[4]-hel-azu** compound, we performed a two-step perturbative analysis (Figure 12). First of all, we study the radical structure, made of fused five-seven-five-membered rings **3**, Figure 12a). This fragment can be seen as the result of the interaction between the pentafulvene derivative **1** and the allyl radical **2**.

The SOMO of the allyl group is less stable than the LUMO of **1**. As a result, the resulting fragment **3** can be viewed as a radical anion pentafulvene derivative paired with an allyl cation. This fragment can then interact with a C_5H_7 radical **4**, Figure 12b). Since the SOMO of C_5H_7 does not have the proper symmetry, the LUMO is the orbital that interacts with the SOMO of fragment **3**. In the singlet ground state, both radicals couple into the HOMO of the **[4]-azu** compound. Formally, one electron is transferred from the C_5H_7 moiety (**4**) to the fragment **3**. Thus, in **[4]-azu** fourteen electrons are shared by the thirteen carbons of the 5-7-5 motif. These fourteen electrons (which are

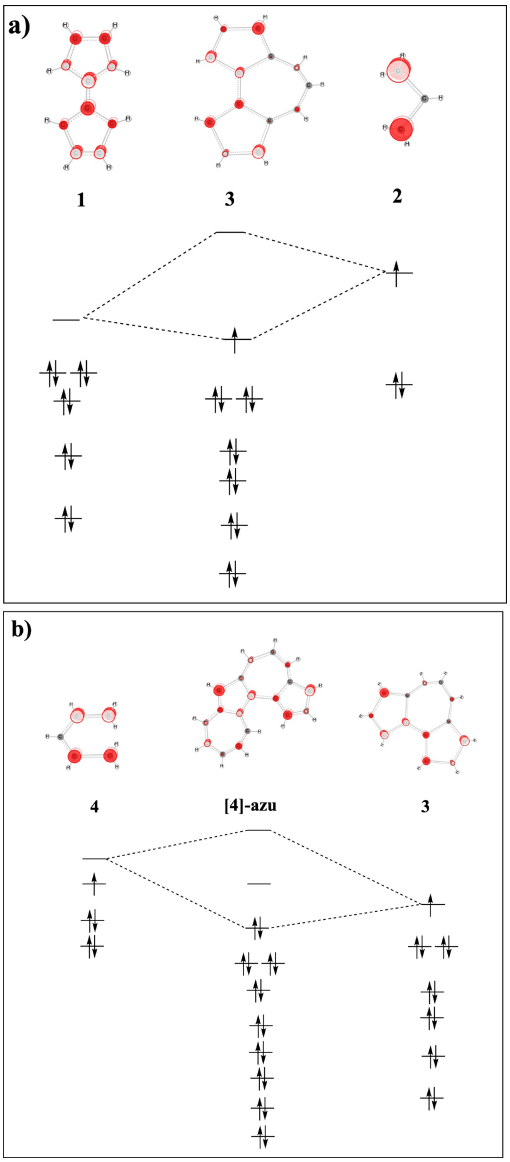

Figure 12. Perturbative analysis based on fragment molecular orbitals: a) π molecular orbital diagram of the five-seven-five-membered fused rings in ortho based on fragment orbitals. b) π molecular orbital diagram of the **[4]-azu**. The interacting Hückel molecular orbitals are represented for 1, 2, 3 and 4 fragments, as well as the HOMO for **[4]-azu**.

aromatic according to Hückel $14 = 4 \times 3 + 2$) are responsible for the aromatic circuit of this 5-7-5 motif in the singlet state of **[4]-azu**. This simple yet powerful fragment molecular orbital approach allows to rationalize the IMS3D maps and the ACID plots of **[4]-azu**. With this approach, it becomes clear why the azulene moiety does not behave as such when it is fused with other azulene moieties. Note that the wave function decomposition for **[4]-azu** also indicates that, in addition to the neutral structures, the ionic ones carry significant weight compared to their analogues, **[4]-hel** and **[4]-hel-azu** (see Supporting Information SI.7). In Figure 7, ψ_5, ψ_9 and ψ_{15} reveal a negative charge on the five-membered rings, in agreement with the electron transfer described previously.

[6]-hel, [6]-hel-azu and [6]-azu

In Figures 13 and 14, similar (anti)-aromatic behavior is observed in **[6]-hel** and **[6]-hel-azu** for both the S_0 and T_1 states, as for the four-ring containing compounds: the azulene moiety behaves as azulene alone, the five-membered ring is more aromatic than the seven-membered ring in the S_0 state, and antiaromaticity appears in the triplet state over the azulene motif. The antiaromatic regions in T_1 aligns well with the areas of the spin density surfaces where spin α predominates over the azulene moiety (see Supporting Information SI.5). We can conclude that the radical is localized over azulene. However, in

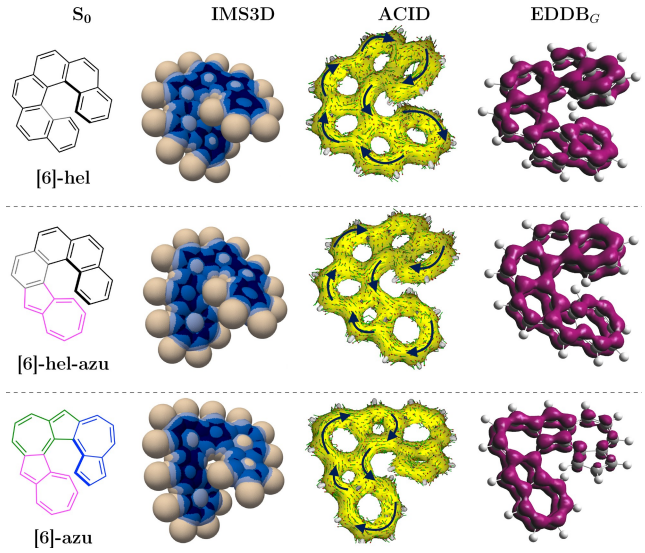

Figure 13. IMS-3D, ACID and EDDB for the singlet ground state of **[6]-hel**, **[6]-hel-azu** and **[6]-azu**. A red arrow indicates a paratropic current, and a blue arrow indicates a diatropic current (see Ref. [68] for high resolution ACID isosurfaces).

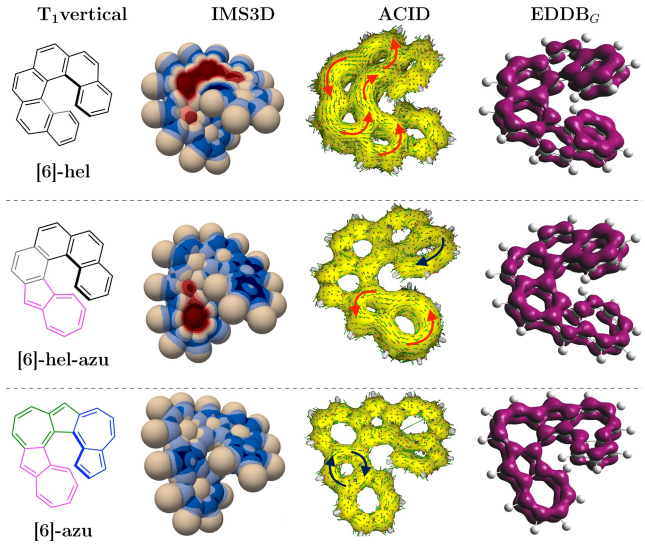

Figure 14. IMS-3D, ACID and EDDB for the vertical triplet state of **[6]-hel**, **[6]-hel-azu** and **[6]-azu**. A red arrow indicates a paratropic current, and a blue arrow indicates a diatropic current (see Ref. [68] for high resolution ACID isosurfaces).

[6]-hel-azu, an aromatic region in the naphthalene unit formed by the A/B rings is clearly identified in the triplet state, this is not the case for **[4]-hel-azu**.

For **[6]-azu**, the strongly aromatic region in S_0 (shown by the dark blue color in its IMS3D map) is noteworthy and corresponds to $18 = 4 \times 4 + 2$ delocalized electrons. This region is also highlighted in the ACID maps by a continuous circuit. Consistently, the same region shows greater wave function delocalization in the EDDB analysis compared to the original azulene unit formed by the A/B rings, which appears to participate less significantly in this delocalization. The T_1 state of **[6]-azu** does not display antiaromatic regions as seen in **[4]-azu**, but instead shows regions with a tendency toward aromaticity, such as the five-membered rings (C and E). While EDDB suggests delocalization across the molecule, the ACID maps for these rings reveal less defined current circuits, likely due to the partial cancellation of opposing induced currents.

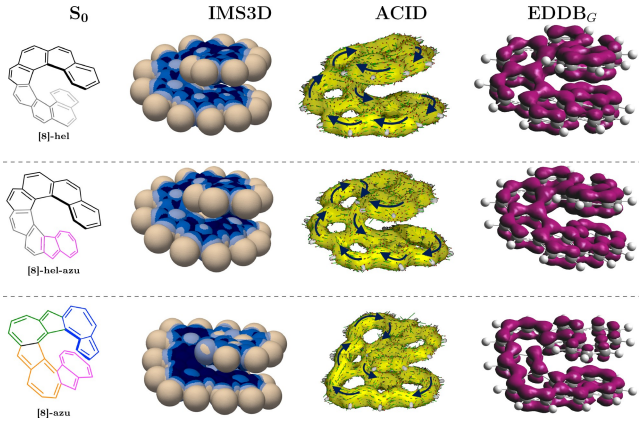

Figure 15. IMS-3D, ACID and EDDB for the singlet ground state of **[8]-hel**, **[8]-hel-azu** and **[8]-azu**. A red arrow indicates a paratropic current, and a blue arrow indicates a diatropic current (see Ref. [68] for high resolution ACID isosurfaces).

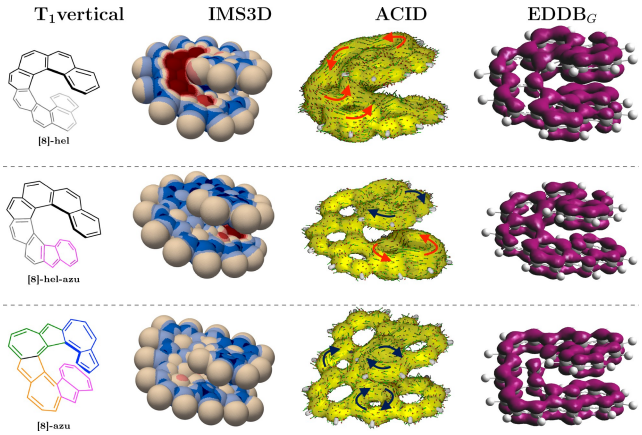

Figure 16. IMS-3D, ACID and EDDB for the vertical triplet state of **[8]-hel**, **[8]-hel-azu** and **[8]-azu**. A red arrow indicates a paratropic current, and a blue arrow indicates a diatropic current (see Ref. [68] for high resolution ACID isosurfaces).

[8]-hel, [8]-hel-azu and [8]-azu

Understanding the behavior of aromaticity in azulene-based helicenes is a great challenge due to the structural complexity involved (Figures 15 and 16). We propose an explanation based on a comparison with its respective analogues analyzed above.

The IMS3D maps show comparable patterns in all compounds to their six-membered ring analogues. In S_0 with an aromaticity extended practically throughout the entire molecule in **[8]-hel** and **[8]-hel-azu**, and **[8]-azu** with the pattern in common with **[6]-azu** of 18π electrons (5-7-5-7 pattern at E/F/G/H rings). ACID also allows us to identify an external circuit in **[8]-hel** and **[8]-hel-azu**, and the 18π electron circuit in **[8]-azu**. EDDB also seems to correspond, showing in this same region a greater density and delocalization of the wave function.

In addition, in T_1 the antiaromaticity located in the azulene motif and aromaticity in the initial phenanthrene motif of the helix in **[8]-hel-azu** still remains. It remains further notable that **[8]-azu**, as in **[6]-azu**, does not reflect azulene behavior as observed in the **[n]-hel-azu** family, instead showing a localized aromatic character in the five-membered ring (as in **[6]-azu**). Also note how the ACID maps show electron circulations in the antiaromaticity regions in IMS3D maps and **[8]-azu** continues to show its particularity of circulation in the five-membered rings, in the opposite direction to the circuits observed in **[8]-hel** and **[8]-hel-azu**.

As has been observed according to the IMS3D and EDDB maps analyzed, the aromaticity and at the same time the ability of electron delocalization is affected when azulene units are introduced into the molecular system in comparison with benzenoid helicenes. We can affirm that the aromaticity in the ground state decreases in this order: **[n]-hel** > **[n]-hel-azu** > **[n]-azu**. Considering this same order, it can be seen that in the first excited state the antiaromaticity decreases.

Conclusions

In this work, we explore the aromaticity and electron delocalization in azulene-containing [n]-helicenes (n = 4,6,8). After we demonstrate that these metastable compounds are likely to be synthesized, as they represent minima on the potential energy surface with high isomerization barriers, we examine their ground- and triplet-excited-state wavefunctions, with a focus on electron delocalization and aromaticity when applicable. We find that the incorporation of the azulene moiety introduces ionic and radical character into the wavefunction. We show that the introduction of azulene inside the helicenes leads to charge separation in the ground state, which does not appear in the triplet-excited state. Additionally, we find that in smaller helicenes, the azulene pattern behaves similarly to isolated azulene. However, for helicenes with more than six rings, a new pattern emerges that can be understood on the basis of the interaction between molecular fragments. We believe that this study will contribute to a deeper understanding of the electronic structure of modified helicenes and inspire further efforts to synthesize such compounds.

Acknowledgements

The authors acknowledge the Ministère de l'éducation nationale for funding the Ph.D. of Amisadai Lorenzo Reyes. We thank also the Université Cheikh Anta Diop together with Aix-Marseille Université for funding Fatim Ndeye Ndiaye. Centre de Calcul Intensif d'Aix-Marseille is acknowledged for granting access to its high performance computing resources. This work was funded, in part, by the Agence Nationale de la Recherche (ANR, grant ANR-19-CE07-0041). A. A. acknowledges the Spanish Ministerio de Universidades and the EU for a complementary Margarita Salas grant (REQ2021_A_02) and European Union's Framework Programme for Research and Innovation Horizon Europe under the Marie Skłodowska-Curie Grant Agreement No. 101106492 (project title: Full-Fission).

Conflict of Interests

The authors declare no conflict of interest.

Data Availability Statement

The data that support the findings of this study are available from the corresponding author upon reasonable request.

Keywords: excited states · aromaticity · polycyclic aromatic hydrocarbons · azulene · non-benzenoid hydrocarbons

[1] X. Yang, F. Rominger, M. Mastalerz, *Angew. Chem. Int. Ed.* **2019**, *58*, 17577.
[2] H. Xin, B. Hou, X. Gao, *Acc. Chem. Res.* **2021**, *54*, 1737.
[3] A. Ong, T. Tao, Q. Jiang, Y. Han, Y. Ou, K.-W. Huang, C. Chi, *Angew. Chem. Int. Ed.* **2022**, *61*, e202209286.
[4] Y. Liang, S. Wang, M. Tang, L. Wu, L. Bian, L. Jiang, Z.-B. Tang, J. Liu, A. Guan, Z. Liu, *Angew. Chem. Int. Ed.* **2023**, *135*, e202218839.
[5] P. Mathey, F. Lirette, I. Fernández, L. Renn, R. T. Weitz, J.-F. Morin, *Angew. Chem. Int. Ed.* **2023**, *62*, e202216281.
[6] R. Liu, Y. Fu, F. Wu, F. Liu, J.-J. Zhang, L. Yang, A. A. Popov, J. Ma, X. Feng, *Angew. Chem. Int. Ed.* **2023**, *62*, e202219091.
[7] K. Biswas, Q. Chen, S. Obermann, J. Ma, D. Soler-Polo, J. Melidonie, A. Barragán, A. Sánchez-Grande, K. Lauwaet, J. M. Gallego, R. Miranda, D. Écija, P. Jelínek, X. Feng, J. I. Urgel, *Angew. Chem. Int. Ed.* **2024**, *63*, e202318185.
[8] F. Wu, A. Barragán, A. Gallardo, L. Yang, K. Biswas, D. Écija, J. I. Mendieta-Moreno, J. I. Urgel, J. Ma, X. Feng, *Chem. Eur. J.* **2023**, *29*, e202301739.
[9] C. Duan, J. Zhang, S. Cai, J. Xiang, X. Yang, X. Gao, *Eur. J. Org. Chem.* **2023**, *26*, e202201347.
[10] N. Ogawa, Y. Yamaoka, H. Takikawa, K.-i. Yamada, K. Takasu, *J. Am. Chem. Soc.* **2020**, *142*, 13322.
[11] L. Qin, Y.-Y. Huang, B. Wu, J. Pan, J. Yang, J. Zhang, G. Han, S. Yang, L. Chen, Z. Yin, Y. Shu, L. Jiang, Y. Yi, Q. Peng, X. Zhou, C. Li, G. Zhang, X.-S. Zhang, K. Wu, D. Zhang, *Angew. Chem. Int. Ed.* **2023**, *62*, e202304632.
[12] A. Konishi, M. Yasuda, *Chem. Lett.* **2021**, *50*, 195.
[13] K. Uehara, P. Mei, T. Murayama, F. Tani, H. Hayashi, M. Suzuki, N. Aratani, H. Yamada, *Eur. J. Org. Chem.* **2018**, 4508.
[14] C. Zhu, K. Shoyama, F. Würthner, *Angew. Chem. Int. Ed.* **2020**, *59*, 21505..
[15] H. Xin, B. Hou, X. Gao, *Acc. Chem. Res.* **2021**, *54*, 1737.
[16] T. Okazaki, K. K. Laali, *Org. Biomol. Chem.* **2003**, *1*, 3078.
[17] D. Dunlop, L. Ludvíková, A. Banerjee, H. Ottosson, T. Slanina, *J. Am. Chem. Soc.* **2023** *145*, 21569.
[18] C. Zhang, J. Cheng, Q. Wu, S. Hou, S. Feng, B. Jiang, C. J. Lambert, X. Gao, Y. Li, J. Li, *J. Am. Chem. Soc.* **2023**, *145*, 1617.
[19] C. Yang, W. Q. Tian, *ChemPlusChem* **2023**, *88*, e202300279.
[20] K. Yamamoto, M. Okazumi, H. Suemune, K. Usui, *Org. Lett.* **2013**, *15*, 1806.
[21] M. Narita, T. Teraoka, T. Murafuji, Y. Shiota, K. Yoshizawa, S. Mori, H. Uno, S. Kanegawa, O. Sato, K. Goto, F. Tani, *Bull. Chem. Soc. Jpn.* **2019**, *92*, 1867.
[22] J. Ma, Y. Fu, E. Dmitrieva, F. Liu, H. Komber, F. Hennersdorf, A. A. Popov, J. J. Weigand, J. Liu, X. Feng, *Angew. Chem. Int. Ed.* **2020**, *59*, 5637.
[23] Y. Han, Z. Xue, G. Li, Y. Gu, Y. Ni, S. Dong, C. Chi, *Angew. Chem. Int. Ed.* **2020**, *59*, 9026.
[24] C. Duan, J. Zhang, J. Xiang, X. Yang, X. Gao, *Angew. Chem. Int. Ed.* **2022**, *61*, e202201494.
[25] C. Duan, H. Xin, X. Gao, *Tetrahedron Lett.* **2023**, *123*, 154553.
[26] Y. Nakai, T. Mori, Y. Inoue, *J. Phys. Chem. A* **2012**, *116*, 7372.
[27] Y.-Y. Ju, H. Luo, Z.-J. Li, B.-H. Zheng, J.-F. Xing, X.-W. Chen, L.-X. Huang, G.-H. Nie, B. Zhang, J. Liu, Y.-Z. Tan, *Angew. Chem. Int. Ed.* **2024**, *136*, e202402621.
[28] W. Niu, Y. Fu, Z.-L. Qiu, C. J. Schürmann, S. Obermann, F. Liu, A. A. Popov, H. Komber, J. Ma, X. Feng, *J. Am. Chem. Soc.* **2023**, *145*, 26824.
[29] M. Cei, L. Di Bari, F. Zinna, *Chirality* **2023**, *35*, 192.
[30] A. Diaz-Andres, J. Marín-Beloqui, J. Wang, J. Liu, J. Casado, D. Casanova, *Chem. Sci.* **2023**, *14*, 6420.
[31] Y. Kalachyova, O. Guselnikova, R. Elashnikov, I. Panov, J. Žádný, V. Církva, J. Storch, J. Sykora, K. Zaruba, V. Švorčík, O. Lyutakov, *ACS Appl. Mater. Interfaces* **2019**, *11*, 1555.
[32] V. Kiran, S. P. Mathew, S. R. Cohen, I. Hernández Delgado, J. Lacour, R. Naaman, *Adv. Mater.* **2016**, *28*, 1957.
[33] T. Mori, *Chem. Rev.* **2021**, *121*, 2373.
[34] T. Li, L. Shen, X. Wang, X. Fan, B. Cui, Y. Chen, B. Yang, H. Liu, X. Li, *J. Mater. Chem. C* **2023**, *11*, 16748.
[35] M. Solà, *Nat. Chem.* **2022**, *14*, 585.
[36] G. Merino, M. Solà, I. Fernandez, C. Foroutan-Nejad, P. Lazzeretti, G. Frenking, H. L. Anderson, D. Sundholm, F. Cossio, M. A. Petrukhina, J. Wu, J. Wu, A. Restrepo, *Chem. Sci.* **2023**.
[37] H. Ottosson, *Chem. Sci.* **2023**, *14*, 5542.
[38] M. Solà, Aromaticity: Types, Rules, and Quantification, in M. Yáñez, R. J. Boyd (Editors), *Comprehensive Computational Chemistry First Edition)*, pages 189–209, Elsevier, Oxford, first edition edition **2024**.
[39] M. K. Cyrański, *Chem. Rev.* **2005**, *105*, 3773.
[40] J. Kruszewski, T. M. Krygowski, *Tetrahedron Lett.* **1972**, *13*, 3839.
[41] T. M. Krygowski, *J. Chem. Inf. Comput. Sci.* **1993**, *33*, 70.
[42] P. v R. Schleyer, C. Maerker, A. Dransfeld, H. Jiao, N. J. R. van Eikema Hommes, *J. Am. Chem. Soc.* **1996**, *118*, 6317.
[43] Z. Chen, C. S. Wannere, C. Corminboeuf, R. Puchta, P. v R. Schleyer, *Chem. Rev.* **2005**, *105*, 3842.
[44] M. Giambiagi, M. Segre De Giambiagi, C. D. Dos Santos Silva, A. Paiva De Figueiredo, *Phys. Chem. Chem. Phys.* **2000**, *2*, 3381.
[45] F. Feixas, E. Matito, J. Poater, M. Solà, *J. Comb. Chem.* **2008**, *29*, 1543.
[46] C. Foroutan-Nejad, *J. Org. Chem.* **2023**, *88*, 14831.
[47] A. Artigas, Y. Carissan, D. Hagebaum-Reignier, H. Bock, F. Durola, Y. Coquerel, *Chem. Eur. J.* **2024**, *30*, e202401016..
[48] M. Orozco-Ic, J. Barroso, N. D. Charistos, A. Muñoz-Castro, G. Merino, *Chem. Eur. J.* **2020**, *26*, 326.
[49] D. Inostroza, V. García, O. Yañez, J. J. Torres-Vega, A. Vásquez-Espinal, R. Pino-Rios, R. Báez-Grez, W. Tiznado, *New J. Chem.* **2021**, *45*, 8345.
[50] D. W. Szczepanik, M. Andrzejak, J. Dominikowska, B. Pawełek, T. M. Krygowski, H. Szatylowicz, M. Solà, *Phys. Chem. Chem. Phys.* **2017**, *19*, 28970.
[51] L. Leyva-Parra, R. Pino-Rios, D. Inostroza, M. Solà, M. Alonso, W. Tiznado, *Chem. Eur. J.* **2024**, *30*, e202302415. .
[52] A. Artigas, D. Hagebaum-Reignier, Y. Carissan, Y. Coquerel, *Chem. Sci.* **2021**, *12*, 13092.
[53] A. Artigas, F. Rigoulet, M. Giorgi, D. Hagebaum-Reignier, Y. Carissan, Y. Coquerel, *J. Am. Chem. Soc.* **2023**, *145*, 15084.
[54] F. Aribot, A. Merle, P. Dechambenoit, H. Bock, A. Artigas, N. Vanthuyne, Y. Carissan, D. Hagebaum-Reignier, Y. Coquerel, F. Durola, *Angew. Chem. Int. Ed.* **2023**, *62*, e202304058.
[55] L. Sturm, A. Artigas, Y. Coquerel, I. H. Bechtold, F. Durola, H. Bock, *Angew. Chem. Int. Ed.* **2024**, *63*, e202403170..
[56] F. Full, A. Artigas, K. Wiegand, D. Volland, K. Szkodzińska, Y. Coquerel, A. Nowak-Król, *J. Am. Chem. Soc.* **2024**, *146*, 29245.
[57] D. Geuenich, K. Hess, F. Köhler, R. Herges, *Chem. Rev.* **2005**, *105*, 3758.
[58] J. P. Foster, F. Weinhold, *J. Am. Chem. Soc.* **1980** *102*, 7211.

[59] Y. Carissan, D. Hagebaum-Reignier, N. Goudard, S. Humbel, *J. Phys. Chem. A* **2008**, *112*, 13256.
[60] J. M. Schulman, R. L. Disch, *J. Phys. Chem. A* **1999**, *103*, 6669.
[61] G. Portella, J. Poater, J. M. Bofill, P. Alemany, M. Solà, *J. Org. Chem.* **2005**, *70*, 4560.
[62] M. J. Frisch, G. W. Trucks, H. B. Schlegel, G. E. Scuseria, M. A. Robb, J. R. Cheeseman, G. Scalmani, V. Barone, G. A. Petersson, H. Nakatsuji, X. Li, M. Caricato, A. V. Marenich, J. Bloino, B. G. Janesko, R. Gomperts, B. Mennucci, H. P. Hratchian, J. V. Ortiz, A. F. Izmaylov, J. L. Sonnenberg, D. Williams-Young, F. Ding, F. Lipparini, F. Egidi, J. Goings, B. Peng, A. Petrone, T. Henderson, D. Ranasinghe, V. G. Zakrzewski, J. Gao, N. Rega, G. Zheng, W. Liang, M. Hada, M. Ehara, K. Toyota, R. Fukuda, J. Hasegawa, M. Ishida, T. Nakajima, Y. Honda, O. Kitao, H. Nakai, T. Vreven, K. Throssell, J. A. Montgomery, Jr., J. E. Peralta, F. Ogliaro, M. J. Bearpark, J. J. Heyd, E. N. Brothers, K. N. Kudin, V. N. Staroverov, T. A. Keith, R. Kobayashi, J. Normand, K. Raghavachari, A. P. Rendell, J. C. Burant, S. S. Iyengar, J. Tomasi, M. Cossi, J. M. Millam, M. Klene, C. Adamo, R. Cammi, J. W. Ochterski, R. L. Martin, K. Morokuma, O. Farkas, J. B. Foresman, D. J. Fox, Gaussiañ16 Revision A.03 **2016**, gaussian Inc. Wallingford CT.
[63] A. D. Becke, E. R. Johnson, *J. Chem. Phys.* **2005**, *123*, 154101.
[64] E. R. Johnson, A. D. Becke, *J. Chem. Phys.* **2006**, *124*, 174104.
[65] S. Grimme, S. Ehrlich, L. Goerigk, *J. Comput. Chem.* **2011**, *32*, 1456.
[66] Y. Carissan, https://github.com/ycarissan/ims3d.py **2021**.
[67] D. W. Szczepanik, M. Andrzejak, K. Dyduch, E. Zak, M. Makowski, G. Mazur, J. Mrozek, *Phys. Chem. Chem. Phys.* **2014**, *16*, 20514.
[68] D. W. Szczepanik, M. Solà, 8 – The Electron Density of Delocalized Bonds (EDDBs) as a Measure of Local and Global Aromaticity, in I. Fernandez (Editor), *Aromaticity*, pages 259–284, Elsevier **2021**
[69] E. D. Glendening, J. K. Badenhoop, A. E. Reed, J. E. Carpenter, J. A. Bohmann, C. M. Morales, P. Karafiloglou, C. R. Landis, F. Weinhold, NBO 7.0, Theoretical Chemistry Institute, University of Wisconsin, Madison.
[70] C. Prud'homme, J.-G. Fages, *J. Open Source Softw.* **2022**, *7*, 4708.
[71] C. Terrioux, https://github.com/Terrioux/pah-tools **2024**.
[72] Y. Carissan, N. Goudard, D. Hagebaum-Reignier, S. Humbel, *J. Phys. Conf. Ser.* **2016**, *738*, 012015.
[73] Supporting Information Data, https://github.com/ycarissan/SI-of-Ground-and-excited-state-aromaticity-in-azulene-based-helicenes **2024**.
[74] M. S. Mirzaei, A. A. Taherpour, C. Wentrup, *J. Org. Chem.* **2022**, *87*, 11503.
[75] M. Dey, D. Ghosh, *J. Phys. Chem. Lett.* **2022**, *13*, 11795.
[76] A. R. Katritzky, M. Karelson, A. P. Wells, *J. Org. Chem.* **1996**, *61*, 1619.
[77] Y. A. Mikheev, L. N. Guseva, Y. A. Ershov, *Russ. J. Phys. Chem.* **2012**, *86*, 1875.
[78] T. Kirschbaum, F. Rominger, M. Mastalerz, *Chem. Eur. J.* **2023**, *29*, e202301470.
[79] R. Báez-Grez, R. P. Rios, *Phys. Chem. Chem. Phys.* **2024**, *26*, 12162.
[80] M. Kędziorek, P. Mayer, H. Mayr, *Eur. J. Org. Chem.* **2009**, 1202.
[81] A. C. Razus, *Symmetry* **2023**, *15*, 310.
[82] Y. Carissan, N. Goudard, D. Hagebaum-Reignier, S. Humbel, HuLiS Program: Lewis embedded in Hückel Theory **2013**, https://www.hulis.free.fr.

Manuscript received: December 10, 2024
Revised manuscript received: January 17, 2025
Accepted manuscript online: January 20, 2025
Version of record online: March 4, 2025